HHS Public Access

Author manuscript

Bioconjug Chem. Author manuscript; available in PMC 2016 October 21.

Published in final edited form as:

Bioconjug Chem. 2015 October 21; 26(10): 2118–2124. doi:10.1021/acs.bioconjchem.5b00414.

Novel Preparation Methods of ^{52}Mn for ImmunoPET Imaging

Stephen A. Graves[†], **Reinier Hernandez**[†], **Jesper Fonslet**[‡], **Christopher G. England**[†], **Hector F. Valdovinos**[†], **Paul A. Ellison**[†], **Todd E. Barnhart**[†], **Dennis R. Elema**[‡], **Charles P. Theuer**[§], **Weibo Cai**[†,||,⊥], **Robert J. Nickles**[†], and **Gregory W. Severin**[‡,*]

[†]Department of Medical Physics, University of Wisconsin – Madison, Madison, Wisconsin 53706, United States

[||]Department of Radiology, University of Wisconsin – Madison, Madison, Wisconsin 53706, United States

[⊥]Carbone Cancer Center, University of Wisconsin – Madison, Madison, Wisconsin 53706, United States

[‡]Technical University of Denmark, Center for Nuclear Technologies, 4000 Roskilde, Denmark

[§]TRACON Pharmaceuticals, San Diego, California 92122, United States

Abstract

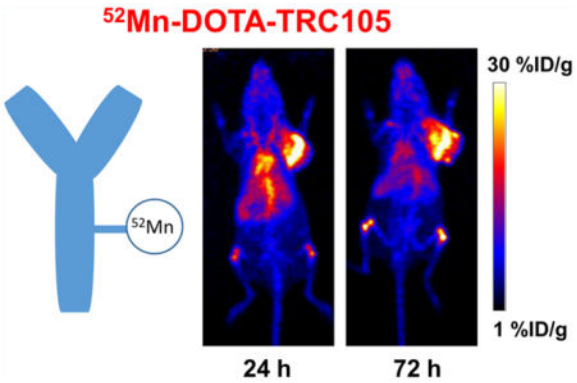

^{52}Mn ($t_{1/2}$ = 5.59 d, β^+ = 29.6%, $E_{\beta ave}$ = 0.24 MeV) shows promise in positron emission tomography (PET) and in dual-modality manganese-enhanced magnetic resonance imaging (MEMRI) applications including neural tractography, stem cell tracking, and biological toxicity studies. The extension to bioconjugate application requires high-specific-activity ^{52}Mn in a state suitable for macromolecule labeling. To that end a ^{52}Mn production, purification, and labeling system is presented, and its applicability in preclinical, macromolecule PET is shown using the conjugate ^{52}Mn-DOTA-TRC105. ^{52}Mn is produced by 60 μA, 16 MeV proton irradiation of

*Corresponding Author: gsev@dtu.dk. Phone: +45 46 77 53 69.

The authors declare the following competing financial interest(s): Charles P. Theuer is an employee of TRACON Pharmaceuticals. The other authors have no competing interests to declare.

Supporting Information

The Supporting Information is available free of charge on the ACS Publications website at DOI: 10.1021/acs.bioconj-chem.5b00414. Dosimetry comparison between ^{89}Zr and ^{52}Mn, including contaminant ^{54}Mn;[32–37] tabulated ex vivo biodistribution data; Derenzo phantom images (PDF)

natural chromium metal pressed into a silver disc support. Radiochemical separation proceeds by strong anion exchange chromatography of the dissolved Cr target, employing a semiorganic mobile phase, 97:3 (v:v) ethanol:HCl (11 M, aqueous). The method is 62 ± 14% efficient (n = 7) in ^{52}Mn recovery, leading to a separation factor from Cr of (1.6 ± 1.0) × 10^6 (n = 4), and an average effective specific activity of 0.8 GBq/μmol (n = 4) in titration against DOTA. ^{52}Mn-DOTA-TRC105 conjugation and labeling demonstrate the potential for chelation applications. In vivo images acquired using PET/CT in mice bearing 4T1 xenograft tumors are presented. Peak tumor uptake is 18.7 ± 2.7%ID/g at 24 h post injection and ex vivo ^{52}Mn biodistribution validates the in vivo PET data. Free $^{52}Mn^{2+}$ (as chloride or acetate) is used as a control in additional mice to evaluate the nontargeted biodistribution in the tumor model.

INTRODUCTION

Interest in ^{52}Mn-based positron emission tomography (PET) applications has increased dramatically in recent years partly due to PET/MRI technological advancements and partly due to increased demand for long-lived PET radiometals such as ^{64}Cu and ^{89}Zr.[1,2] For MRI, the T_1-shortening properties of bulk manganese are employed in manganese-enhanced magnetic resonance imaging (MEMRI). However, the biological toxicity of bulk manganese[3] has hampered the development and progression of otherwise useful applications such as diffusion-tensor neuronal fiber tractography,[4–6] nociceptive activity detection,[7] functional imaging of brain activation,[8] diagnosis and staging of pancreatic cancer,[9] heptocellular carcinoma detection,[10] cell tracking,[11,12] and evaluation of cardiac inotropic therapy.[13] Manganese-52-based PET tracer alternatives may provide analogous data with lower toxicity and thereby promote clinical application.

Additionally, ^{52}Mn may offer advantages over traditional ^{64}Cu or ^{89}Zr immunoPET in situations where treatment response monitoring at late time-points (2–3 weeks) is desired. In cases where radioimmunotherapy is initiated with long-lived nuclides such as ^{177}Lu, the full time-course of treatment could be monitored by ^{52}Mn PET. Further, due to the abundance of coincident high energy gammas, ^{52}Mn is one of relatively few nuclides that can be used in third-gamma coincidence PET for either dual nuclide event tagging or combined Compton telescope PET tomography.[14] Despite this, clinical translation should proceed with caution due to the preponderance of coincident high energy gammas: 744 keV (90%), 935 keV (95%), and 1434 keV (100%). Coupled with the myriad biological roles of manganese, which may lead to prolonged retention of radiomanganese in critical organs, careful dosimetry prior to translation should be considered.

A common method for high-yield production of ^{52}Mn is via the ^{52}Cr(p,n) reaction: a route available using small biomedical cyclotrons.[15–18] Due to the natural 83.8% abundance of ^{52}Cr in ^{nat}Cr and the low propensity for impurity formation of other Mn isotopes during proton irradiation, ^{nat}Cr, which is available in high purity from various distributors, is an inexpensive alternative to enriched target material. The main radionuclidic impurity formed from the irradiation of ^{nat}Cr is ^{54}Mn ($t_{1/2}$ = 312 d) with an energy dependent coproduction rate, representing 0.1–0.4% of the ^{52}Mn activity at the end of a short bombardment at 16

MeV.[16,19] For 1 h 16 MeV irradiations on a thick Cr target, the expected yield of ^{52}Mn is approximately 9.5 MBq/μA.[19]

In order to separate ^{52}Mn from the bulk Cr matrix, anion exchange from semiaqueous hydrochloric acid media is a simple trap-and-release technique. Previously published methods for separating manganese from chromium involving anion exchange rely upon the formation of anionic chloride complexes of manganese.[17,18,20] Notably, there is a marked enhancement in the formation of the anionic manganese chlorides when hydration is limited by using nonaqueous solvents.[21] However, under similar conditions Cr^{3+} does not form anionic chloride complexes. This behavior is evident in the distribution coefficients for Mn and Cr against anion exchange resin from 97% EtOH 0.3 M HCl solutions,[21] where the resin affinities are sufficiently disparate for trap-and-release purification of ^{52}Mn from bulk Cr with small resin beds.

As a first test for bifunctional chelation of Mn to macromolecules, the common chelate DOTA (1,4,7,10 tetraazacyclododecane 1,4,7,10 tetraacetic acid) is an obvious choice due to its ubiquity in radiochemical applications and the reported stability of DOTA chelates with Mn(II).[22] Because the long physical half-life of ^{52}Mn ($t_{1/2}$ = 5.591 days[23]) lends itself well to the long biological circulation times in radioimmunoPET applications, a demonstration of the stable chelation of ^{52}Mn using bifunctionalized DOTA conjugated to a monoclonal antibody proves its usefulness as a radiotracer. For this study, TRC105, a chimeric human/murine immunoglobulin G (IgG_1) monoclonal antibody (mAb) which binds to the angiogenic marker CD105 with very high specificity, was chosen as the model compound due to the extensive body of data available that describes its biodistribution with other radiometals and chelates.[24–26] This antibody is currently associated with 17 phase I and II multicenter clinical trials which are planned, underway, or already completed, investigating the therapeutic efficacy in a variety of solid tumors either alone or as an adjunct to other treatment techniques.

The purpose of this report is to describe a methodology for the production and purification of ^{52}Mn that is amenable to bioconjugate chemistry. A simple cyclotron target made of chromium metal is described, and the procedure for extracting ^{52}Mn from the Cr matrix is given. The chemical purity of the produced ^{52}Mn is demonstrated by trace metal analysis and chelation with DOTA. Finally, the suitability of DOTA as a bifunctional chelate for Mn is investigated by in vivo experiments of ^{52}Mn-DOTA-TRC105 in 4T1 xenograft-bearing mice, and comparison with the biodistribution of weakly coordinated $^{52}Mn^{2+}$. To our knowledge, the formation of ^{52}Mn-DOTA-TRC105 constitutes the first bioconjugate radiomanganese PET agent, and acts as a benchmark of the purity of ^{52}Mn required for targeted PET.

RESULTS AND DISCUSSION

Target Fabrication, Irradiation, Dissolution, and Column Separation

The goal of creating a simple design for metallic chromium irradiation was met by pressing high-purity chromium with a hydraulic press into a silver backing at 30 kN. The Cr/Ag pressed targets were remarkably resilient, withstanding 60 μA of 16 MeV protons for 2 h

without failure. An example target is shown in Figure 1. Based on the alloying behavior of chromium and silver,[27] we speculate that in addition to any mechanical bonding, 30 kN may be sufficient to form an eutectic alloy at the boundary between the two metals facilitating thermal conduction and physical stability. The average end-of-bombardment ^{52}Mn yield was 5 ± 1 MBq/μAh (n = 12), which is approximately half of our previously measured thick target production rate of 9.5 ± 1 MBq/μAh[19] due to target thickness irregularities and partial beam-spot coverage.

Following irradiation, targets were etched with HCl and the resulting solution was diluted with ethanol. This was done in order to reach a condition where dissolved Mn(II) anionic chloride complexes extract onto strong anion-exchange resin while hydrated Cr^{3+} passes through. Upon switching to a fully aqueous 6 M HCl solution ^{52}Mn was released from the resin bed. The entire procedure of trap-and-release, alternating from ethanolic to aqueous mixtures was repeated three times on three separate small AG-1 × 8 columns.

^{52}Mn extraction from ethanolic HCl onto AG-1 × 8 was 73 ± 13%, 91 ± 4%, and 92 ± 5% efficient (n = 7) at each of the column passes. The low first-step separation efficiency is likely due to a lower ethanol concentration, approximately 95%, compared to the ideal concentration of >97% ethanol. It is likely that ^{52}Mn trapping could be greatly improved by drying the dissolved target material before reconstituting in 0.3 M HCl, 97% EtOH. Alternatively, a hydrogen chloride ethanol or dioxane solution (4.0 M HCl in dioxane, Sigma-Aldrich Inc.) could be used after target dissolution to obtain the desired HCl concentration without the burden of added aqueous volume. The overall ^{52}Mn recovery efficiency of 62 ± 14% (n = 7) was sufficient for our purposes, as it was nearly twice as efficient as the previously reported trioctylamine based extraction approach to ^{52}Mn/^{nat}Cr separation[19] and more easily lends itself to automation.

Chromium content in the eluted fractions fell successively at each step by factors of 601 ± 31, 80 ± 6, and 42 ± 5 (n = 1), as seen in Table 1. The overall chromium separation factor was (1.6×10^6) ± (1.0×10^6) (n = 4) as measured by trace metal analysis. During the first column separation, the resin became uniformly green-tinted indicating a slight retention of Cr^{3+}. This chromium did not wash off of the resin in any appreciable way with repeated rinses of the ethanolic HCl. However, upon elution of ^{52}Mn, this species of Cr also coeluted to a small degree. Similar effects were observed in the other two subsequent column separations by tracing the Cr content with microwave plasma atomic emission spectrometry (MP-AES). Surprisingly this behavior contrasts with the published distribution coefficients of Pietrzyk et al., in that the extracted species of Cr was not behaving chromatographically.[21] This is ultimately the reason three sequential separations were required to achieve the necessary purity for labeling, rather than repeated washings. The act of removing the Cr from the column and then reconstituting it in the ethanolic solutions appeared to reset the Cr form dichotomy, although with diminishing returns. This is likely due to the formation of different hydration states of Cr^{3+} in solution and their slow interchange.[28] Regardless, the two additional column repetitions were not restrictive to rapid isolation of the product ^{52}Mn.

Analysis of Purity: Chelation and Trace Metal Quantification

Titration of the ^{52}Mn sample against varying concentrations of DOTA resulted in an effective specific activity of up to 2GBq/μmol. MP-AES trace metal analysis of the final samples are given in Table 2. If all transition metal impurities are considered to be competitive for DOTA chelation, reactions at a level of about 4 GBq/μmol are predicted from the data. It is probable that a significant portion of the trace metal impurities come from the large volumes of ethanol involved in the separation process. For example, we observed iron in the ethanol stock at a concentration of 31 ng/mL, or roughly 5 μg total iron mass in a typical production. An additional in-house distillation of commercial ethanol might be effective in producing metal-free ethanol, reducing impurities in future ^{52}Mn productions.

TRC105 Conjugation, Labeling, Imaging, And Biodistribution

A lower average ^{52}Mn-DOTA effective specific activity of 0.8 GBq/μmol compared to that of the typical ^{89}Zr-DFO assay (~30 GBq/μmol) motivated an increase in the bifunctional-chelate to antibody ratio (25:1) during conjugation. The resulting DOTA-TRC105 had excellent radiolabeling properties as shown in Table 3. 4 μg/MBq of DOTA-TRC105 was sufficient to reach ^{52}Mn complexation efficiencies greater than 95% after 60 min at 37 °C

Injections of ^{52}Mn-DOTA-TRC105 were administered to Balb/c mice bearing 4T1 xenografts and PET data were collected. Maximum intensity projection (MIP) PET images are shown in Figure 2. ROI quantification of the ^{52}Mn-DOTA-TRC105 PET images yielded the time activity curves shown in Figure 3. Finally, the ex vivo biodistribution results shown in Figure 4 confirm the accuracy of image-based ROI quantification.

Tumor uptake peaked at the 24 h PET time-point with an average value of 19 ± 3%ID/g (n = 3). The ^{52}Mn-DOTA-TRC105 time activity curves measured in this work agree well with those seen with ^{89}Zr-labeled TRC105 via desferrioxamine in the same animal and xenograft model[25] indicating a stable conjugate. Furthermore, the increased DOTA conjugation ratio does not seem to perturb CD105 binding affinity. When comparing the ex vivo biodistribution of ^{89}Zr-DF-TRC105 to ^{52}Mn-DOTA-TRC105 the most significant difference is the slower blood clearance rate of ^{52}Mn-DOTA-TRC105 to ^{89}Zr-Df-TRC105. Assuming the same conjugate distribution, dosimetrically, ^{52}Mn is less favorable for injection compared to ^{89}Zr for immunoPET (see Supporting Information). However, in some instances the higher dose from ^{52}Mn may be justified for longer-term scanning, or its use in novel triple coincidence PET cameras.

Comparing ^{52}Mn-DOTA-TRC105 with the “Free ^{52}Mn” PET images, there are clear differences in the distribution pattern. (Note: No qualitative differences were observed between subjects injected with $^{52}MnCl_2$ (n = 2) vs ^{52}Mn-Acetate (n = 2), suggesting rapid ionic dissociation postinjection. These four subjects were therefore combined into a single “Free ^{52}Mn” group.) The most pronounced differences include a lack of thyroid uptake in the ^{52}Mn-DOTA-TRC105 images, and a lack of tumor uptake in the $^{52}MnCl_2$ images. These features support that the DOTA chelation of ^{52}Mn is stable, even 120 h postinjection. However, there is an enhanced signal in the bones with the targeted injections, but not in the

free-ion case. Typically bone uptake in immunoPET is associated with instability of the metal–chelate pair. If this is the case in the present study, it is clear that the slow-dissociating manganese displays a pharmacokinetic profile that is distinct from the free manganese. One possible explanation is a direct interaction between the bone and the DOTA-bound manganese rather than a hydrolysis mechanism for chelate instability. Further investigation into the in vivo behavior of manganese salts may help determine the impact that slow dissociation has upon PET quantification, as has been done for ^{89}Zr.[29]

Impurities

Prior to translation there are many important considerations, especially concerning radionuclidic and chemical purity. The injections in this study contained approximately 0.5% radionuclidic impurity from ^{54}Mn, which contributes only in a small way to personal dosimetry (see Supporting Information), but the long half-life (biological and physical) may be an important factor in deciding whether or not to use enriched ^{52}Cr as an alternative target material: thereby eliminating production of ^{54}Mn. Chemically, the use of chromium in a pharmaceutical production may raise concerns of toxic effects. However, the amount of Cr that remains after purification is extremely low, at most 1 μg for an entire production (150–250 MBq). This Cr has no propensity to form a stable complex with functionalized DOTA[30] and would be further removed during the size-exclusion purification step. For comparison, the EPA reference dose, RfD, for Cr(IV), below which no effects are observed is 3 μg/kg in rats:[31] a level much higher than would be reached following injection of a purified ^{52}Mn-immunoconjugate.

CONCLUSION

The results above and methodology below are intended to provide an easily reproducible path toward investigating bioconjugate systems using ^{52}Mn. The example of ^{52}Mn-DOTA-TRC105 shows that stable chelation of manganese via bifunctionalized DOTA is suitable for tracing macromolecules with PET over the course of several days, with imaging characteristics that compare favorably to ^{89}Zr. Additionally, the effective specific activity of ^{52}Mn that results from anion-exchange separations from ethanol–HCl mixtures is sufficient to conduct antibody imaging.

EXPERIMENTAL PROCEDURES

Materials

All reagents were obtained from commercial vendors and were used as received unless otherwise stated. TRC105 (mAb) was provided by TRACON Pharmaceuticals Inc. 4T1 murine breast cancer cells were obtained from the American Type Culture Collection (ATCC). Aqueous solutions were constituted in >18 MΩ/cm water. Unless noted, the term HCl refers to 32–35% aqueous hydrochloric acid. Ethanol–HCl mixtures were made in v:v proportion using ethanol (molecular biology grade, Sigma-Aldrich) and 32–35% aqueous HCl (untitrated, Optima grade, VWR).

Target Fabrication, Irradiation, Dissolution, and Column Separation

Targets were constructed by placing a natural chromium pellet (99.999% pure, approximately 750 mg, GFS Chemicals) on the center of a 19-mm-diameter 2-mm-thick silver disc (>99.9% pure, Noble Metals, Sarasota, FL) before being wrapped in niobium foil and hydraulically pressed with a force of approximately 30 kN for ten seconds. This force was sufficient to imbed the chromium metal into the silver disc without compromising the integrity of the rear target face. These targets were irradiated by 16 MeV protons (GE PETtrace) with beam currents up to 60 μA.

Following irradiation, targets were etched by 2 mL of HCl (32–35%, Optima, VWR) at 75 °C for 1 h, or until cessation of bubbling (typically 400 mg of the 750 mg Cr target was dissolved by this procedure). The solution was quantitatively transferred to a large centrifuge tube using a 47.5 mL rinse of ethanol (molecular biology grade, Sigma-Aldrich). To this solution, 0.5 mL of HCl was added resulting in a final target solution of 50 mL.

Three columns were constructed, each containing approximately 250 mg of dry AG-1 × 8 strong anion exchange resin (Bio-Rad Laboratories) and were equilibrated and rinsed with 10 mL of 97:3 ethanol–HCl. The 50 mL of target solution was passed through the first column trapping the ^{52}Mn and letting the bulk ^{nat}Cr pass through. After rinsing with 10 mL of 97:3 ethanol–HCl the activity was eluted in 1 mL of 6 M HCl. The eluted volume was diluted to 50 mL with ethanol, and then loaded on the second column. After rinsing, the activity was again eluted in 1 mL of 6 M HCl and taken up to 50 mL with ethanol. With the activity loaded onto the third and final purification column, the column was rinsed, dried with air, and the activity was eluted in approximately 1 mL of 0.1 M of HCl. Due to mobile-phase retention in the resin, invariably the final elution contained ethanol. It should be noted that for some labeling procedures, the eluted product should be dried down and reconstituted in 0.1 M HCl or an appropriate buffer.

Trace Metal Analysis, and DOTA Chelation

An aliquot of ^{52}Mn from each production was taken to dryness under vacuum and reconstituted in a known volume of 0.1 M HCl. Trace concentrations of Cr, Mn, Fe, Co, Ni, Cu, and Zn were measured by microwave plasma atomic emission spectrometry (MP-AES, Agilent). Total metal impurity load for each production was calculated by dividing the sample masses by the fraction of the total activity used for this assay.

For chelation assays, 200 μL of ^{52}Mn activity in 0.1 M HCl was added to 600 μL of pH 4.5, 0.25 M NaOAc buffer. Vials containing 100 μL of increasing DOTA (Macrocyclics Inc.) concentrations were prepared ranging from 0 μg/mL to 10 μg/ mL in water. A 100 μL aliquot of the buffered activity solution was added to each DOTA vial. Vials were vortexed, and left to complex at room temperature for 1 h. Each sample was spotted on a thin layer chromatography (TLC) silica plate (60G F254, Merck KGaA) and was run with 0.25 M NH_4OH mobile phase. This method left unbound activity at the origin and moved ^{52}Mn-DOTA with the mobile phase. RadioTLC's were quantified by phosphor-storage plate autoradiography (Cyclone Plus, PerkinElmer Inc.).

Preparation of the "Free $^{52}Mn^{2+}$" Injections

Eluted ^{52}Mn fractions were taken to dryness under reduced atmosphere at 70 °C to remove acidity and EtOH contamination. $^{52}MnCl_2$ injections were prepared by reconstituting the dried ^{52}Mn in phosphate-buffered saline and ^{52}Mn-Acetate injections were prepared by reconstituting the dried ^{52}Mn in pH 7.5 0.1 M sodium acetate.

DOTA-TRC105 Conjugation and ^{52}Mn Labeling

A solution containing TRC105 was adjusted to pH 8.5–9.0 with 0.1 M Na_2CO_3. p-SCN-Bn-DOTA (Macrocyclics) previously dissolved in DMSO was added to this solution in a 25:1 (DOTA:TRC105) molar ratio. Following this addition, the pH was measured and adjusted to pH 8.5–9.0 with Na_2CO_3. The conjugation reaction was allowed 2 h to complete at room temperature before DOTA-TRC105 was purified by size exclusion chromatography (PD-10, GE-Healthcare) using phosphate-buffered saline (PBS) mobile phase.

75–110 MBq of ^{52}Mn in ~200 μL 0.1 M HCl was added to 500 μL 0.1 M pH 4.5 sodium acetate. To determine the appropriate quantity of DOTA-TRC105, labeling was initially tested with 2.7, 6.8, 13.5, and 27.0 μg/MBq. ^{52}Mn labeling with these samples was monitored by radio-TLC using 50 mM pH 4.5 ethylenediamineetetraacetic acid (EDTA) mobile phase over the course of 1 h at room temperature. TLC peak discrimination was used to distinguish between bound and unbound ^{52}Mn, and peak integration was used for quantification following a background subtraction.

For animal experiments, 4 μg of DOTA-TRC105 per MBq ^{52}Mn was added to the buffered activity solution and allowed to react for 60 min at 37 °C. After labeling, EDTA was added such that the resulting concentration was 1 mM. Labeling yield was quantified by radio-TLC, and the ^{52}Mn-DOTA-TRC105 was purified by size exclusion chromatography using PBS mobile phase. The resulting fraction was collected and passed through a 0.2 μm syringe filter prior to in vivo experiments.

Murine 4T1 Tumor Cell Line and Animal Model

4T1 cells were cultured in RPMI 1640 growth medium (Invitrogen) with 1× low serum growth supplement. During culturing, cells were incubated at 37 °C with 5% CO_2. Once cells reached approximately 75% confluence, they were used for in vivo experiments.

All animal studies were conducted under a protocol approved by the University of Wisconsin Institutional Animal Care and Use Committee. Tumors were established in four- to five-week-old female Balb/c mice purchased from Harlan Sprague–Dawley Inc. by subcutaneous injection of approximately 2×10^6 cells, suspended in 100 μL of 1:1 mixture of RPMI 1640 and Matrigel (BD Biosciences), into the front flank of seven mice. Tumor sizes were monitored, and mice were used for imaging experiments when the diameter of tumors reached 5–8 mm (typically 1–2 weeks after inoculation).

Imaging and Biodistribution Studies

Mice were anesthetized with 2% isofluorane and 2.2–4.4 MBq of ^{52}Mn-DOTA-TRC105 (n = 3), $^{52}MnCl_2$ (n = 2), or ^{52}Mn-Acetate (n = 2) was injected by tail vein in a rapid bolus.

PET/CT imaging was performed (Inveon microPET/CT, Siemens Inc.) at five time-points between 4 and 128 h in the ^{52}Mn-DOTA-TRC105 group, and five time-points between 4 and 96 h in the $^{52}Mn^{2+}$ control groups with at least 40 million coincident counts per PET acquisition. Static images were reconstructed using three-dimensional ordered subset expectation maximization (OSEM3D).

Following the last PET time-point, each animal was sacrificed. In addition to a blood draw, samples from the following tissues were extracted, washed in saline, and weighed: 4T1 tumor, skin, muscle, bone (femur, inferior half), heart, lung, liver, kidney, spleen, pancreas, stomach, intestine, tail, brain, and thyroid. ^{52}Mn activity in each sample was measured by gamma counting (Wizard 2480, PerkinElmer).

The results of both PET region of interest (ROI) and ex vivo biodistribution quantitative analysis were expressed as percent of the injected dose per gram of tissue (%ID/g ± SD).

Supplementary Material

Refer to Web version on PubMed Central for supplementary material.

Acknowledgments

We are grateful to Dr. Andreas Maurer at the University of Tübingen for sharing his experiences with DOTA-Mn reaction conditions. The authors acknowledge and are thankful for their funding from the University of Wisconsin - Madison, the DOE (DE-FG02-12ER41882), the National Science Foundation (DGE-1256259), the National Institutes of Health (5T32GM08349, 5 T32 CA009206-34, NIBIB/NCI 1R01CA169365, and P30CA014520), the American Cancer Society (125246-RSG-13-099-01-CCE), and the EU FP7 framework (MATHIAS).

References

1. Deri MA, Zeglis BM, Francesconi LC, Lewis JS. PET imaging with ^{89}Zr: From radiochemistry to the clinic. Nucl Med Biol. 2013; 40:3–14. [PubMed: 22998840]
2. Wadas TJ, Wong EH, Weisman GR, Anderson CJ. Coordinating radiometals of copper, gallium, indium, yttrium, and zirconium for PET and SPECT imaging of disease. Chem Rev. 2010; 110:2858–2902. [PubMed: 20415480]
3. Crossgrove J, Zheng W. Manganese toxicity upon overexposure. NMR Biomed. 2004; 17:544–553. [PubMed: 15617053]
4. Pirko I, Gamez J, Shearier E, Raman M, Johnson A, Macura S. Manganese Enhanced MRI (MEMRI) in Murine CNS Inflammatory Disease Models (S21. 007). Neurology. 2012; 78:S21.007.
5. Yamada M, Momoshima S, Masutani Y, Fujiyoshi K, Abe O, Nakamura M, Aoki S, Tamaoki N, Okano H. Diffusion-Tensor Neuronal Fiber Tractography and Manganese-enhanced MR Imaging of Primate Visual Pathway in the Common Marmoset: Preliminary Results. Radiology. 2008; 249:855–864. [PubMed: 19011185]
6. Napieczynska, H.; Calaminus, C.; Severin, GW.; Fonslet, J.; Pichler, BJ. Mn-52 as a PET Neural Tract Tracer, abstract # 301, European Molecular Imaging Meeting; March 19, 2015; Tuebingen, Germany. 2015.
7. Jacobs KE, Behera D, Rosenberg J, Gold G, Moseley M, Yeomans D, Biswal S. Oral manganese as an MRI contrast agent for the detection of nociceptive activity. NMR Biomed. 2012; 25:563–569. [PubMed: 22447731]
8. Lin YJ, Koretsky AP. Manganese ion enhances T1–weighted MRI during brain activation: An approach to direct imaging of brain function. Magn Reson Med. 1997; 38:378–388. [PubMed: 9339438]

9. Schima W, Függer R, Schober E, Oettl C, Wamser P, Grabenwöger F, Ryan JM, Novacek G. Diagnosis and Staging of Pancreatic Cancer: Comparison of Mangafodipir Trisodium—Enhanced MR Imaging and Contrast-Enhanced Helical Hydro-CT. AJR, Am J Roentgenol. 2002; 179:717–724. [PubMed: 12185052]
10. Murakami T, Baron RL, Peterson MS, Oliver J 3rd, Davis PL, Confer SR, Federle MP. Hepatocellular carcinoma: MR imaging with mangafodipir trisodium (Mn-DPDP). Radiology. 1996; 200:69–77. [PubMed: 8657947]
11. Kim T, Momin E, Choi J, Yuan K, Zaidi H, Kim J, Park M, Lee N, McMahon MT, Quinones-Hinojosa A. Mesoporous silica-coated hollow manganese oxide nanoparticles as positive T 1 contrast agents for labeling and MRI tracking of adipose-derived mesenchymal stem cells. J Am Chem Soc. 2011; 133:2955–2961. [PubMed: 21314118]
12. Gilad AA, Walczak P, McMahon MT, Na HB, Lee JH, An K, Hyeon T, van Zijl P, Bulte JW. MR tracking of transplanted cells with “positive contrast” using manganese oxide nanoparticles. Magn Reson Med. 2008; 60:1–7. [PubMed: 18581402]
13. Hu TCC, Pautler RG, MacGowan GA, Koretsky AP. Manganese–enhanced MRI of mouse heart during changes in inotropy. Magn Reson Med. 2001; 46:884–890. [PubMed: 11675639]
14. Lang C, Habs D, Parodi K, Thirolf P. Sub-millimeter nuclear medical imaging with high sensitivity in positron emission tomography using β+ coincidences. J Instrum. 2014; 9:P01008.
15. Topping, GJ. PhD Thesis. University of British Columbia; Vancouver, Canada: Feb. 2014 Manganese imaging with positron emission tomography, autoradiography, and magnetic resonance. 2014
16. Wooten AL, Lewis BC, Lapi SE. Cross-sections for (p, x) reactions on natural chromium for the production of $^{52, 52m, 54}$Mn radioisotopes. Appl Radiat Isot. 2015; 96:154–161. [PubMed: 25497324]
17. Topping GJ, Schaffer P, Hoehr C, Ruth TJ, Sossi V. Manganese-52 positron emission tomography tracer characterization and initial results in phantoms and in vivo. Med Phys. 2013; 40:042502. [PubMed: 23556918]
18. Buchholz M, Spahn I, Scholten B, Coenen HH. Cross-section measurements for the formation of manganese-52 and its isolation with a non-hazardous eluent. Radiochim Acta. 2013; 101:491–499.
19. Lewis CM, Graves SA, Hernandez R, Valdovinos HF, Barnhart TE, Cai W, Meyerand ME, Nickles RJ, Suzuki M. ^{52}Mn production for PET/MRI tracking of human stem cells expressing divalent metal transporter 1 (DMT1). Theranostics. 2015; 5:227. [PubMed: 25553111]
20. Daube M, Nickles R. Development of myocardial perfusion tracers for positron emission tomography. Int J Nucl Med Biol. 1985; 12:303–314. [PubMed: 3878834]
21. Pietrzyk, DJ. Retrospective Theses and Dissertations Paper 2390. Iowa State University; 1960. Anion Exchange Separations of Metal Ions in Partially Nonaqueous Solutions.
22. Bianchi A, Calabi L, Giorgi C, Losi P, Mariani P, Palano D, Paoli P, Rossi P, Valtancoli B. Thermodynamic and structural aspects of manganese (II) complexes with polyaminopoly-carboxylic ligands based upon 1, 4, 7, 10-tetraazacyclododecane (cyclen). Crystal structure of dimeric [MnL] 2· 2CH 3 OH containing the new ligand 1, 4, 7, 10-tetraazacyclododecane-1, 4-diacetate. J Chem Soc, Dalton Trans. 2001:917–922.
23. Huo J, Huo S, Ma C. Nuclear data sheets for A= 52. Nucl Data Sheets. 2007; 108:773–882.
24. Engle JW, Hong H, Zhang Y, Valdovinos HF, Myklejord DV, Barnhart TE, Theuer CP, Nickles RJ, Cai W. Positron emission tomography imaging of tumor angiogenesis with a ^{66}Ga-labeled monoclonal antibody. Mol Pharmaceutics. 2012; 9:1441–1448.
25. Hong H, Severin GW, Yang Y, Engle JW, Zhang Y, Barnhart TE, Liu G, Leigh BR, Nickles RJ, Cai W. Positron emission tomography imaging of CD105 expression with ^{89}Zr-Df-TRC105. Eur J Nucl Med Mol Imaging. 2012; 39:138–148. [PubMed: 21909753]
26. Zhang Y, Hong H, Engle JW, Bean J, Yang Y, Leigh BR, Barnhart TE, Cai W. Positron Emission Tomography Imaging of CD105 Expression with a ^{64}Cu-Labeled Monoclonal Antibody: NOTA Is Superior to DOTA. PLoS One. 2011; 6:e28005. [PubMed: 22174762]
27. Venkatraman M, Neumann JP. The Ag-Cr (Silver-Chromium) system. Bull Alloy Phase Diagrams. 1990; 11:263–265.
28. Knox K. Fast and slow reactions of chromium compounds. J Chem Educ. 1990; 67:700.

29. Severin GW, Jorgensen JT, Wiehr S, Rolle AM, Hansen AE, Maurer A, Hasenberg M, Pichler B, Kjaer A, Jensen AI. The impact of weakly bound ^{89}Zr on preclinical studies: non-specific accumulation in solid tumors and aspergillus infection. Nucl Med Biol. 2015; 42:360–368. [PubMed: 25583221]

30. Asti M, Tegoni M, Farioli D, Iori M, Guidotti C, Cutler CS, Mayer P, Versari A, Salvo D. Influence of cations on the complexation yield of DOTATATE with yttrium and lutetium: a perspective study for enhancing the ^{90}Y and ^{177}Lu labeling conditions. Nucl Med Biol. 2012; 39:509–517. [PubMed: 22172388]

31. Agency, U. S. E. P. Integrated Risk Information System (IRIS) on Chromium VI. National Center for Environmental Assessment, Office of Research and Development; Washington, DC: 1999.

32. Ishinishi N, Morishige T. A Study on the Distribution of ^{95}Zr-^{95}Nb Administered Subcutaneously to Rats: Comparison between Young and Adult Rats. J Radiat Res. 1969; 10:101–106. [PubMed: 5382975]

33. O'Neal SL, Hong L, Fu S, Jiang W, Jones A, Nie LH, Zheng W. Manganese accumulation in bone following chronic exposure in rats: Steady-state concentration and half-life in bone. Toxicol Lett. 2014; 229:93–100. [PubMed: 24930841]

34. Greiter MB, Giussani A, Höllriegl V, Li WB, Oeh U. Human biokinetic data and a new compartmental model of zirconium—A tracer study with enriched stable isotopes. Sci Total Environ. 2011; 409:3701–3710. [PubMed: 21724239]

35. Mealey J. Turn-over of carrier-free zirconium-89 in man. Nature. 1957; 179:673–674. [PubMed: 13418761]

36. Mahoney JP, Small WJ. Studies on manganese: III. The biological half-life of radiomanganese in man and factors which affect this half-life. J Clin Invest. 1968; 47:643. [PubMed: 5637148]

37. Stabin MG, Sparks RB, Crowe E. OLINDA/ EXM: the second-generation personal computer software for internal dose assessment in nuclear medicine. J Nucl Med. 2005; 46:1023–1027. [PubMed: 15937315]

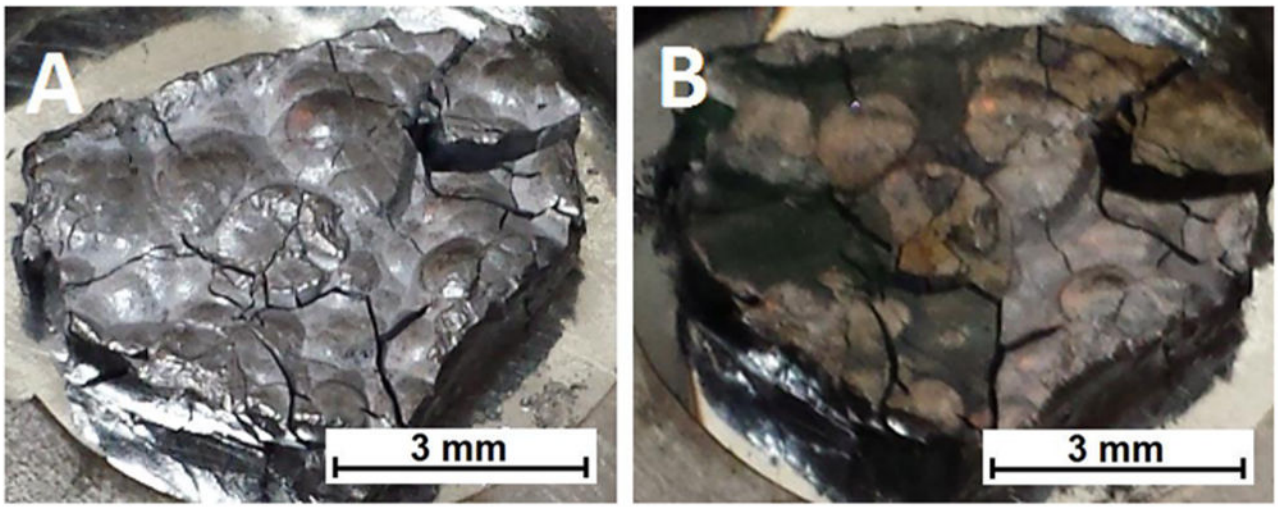

Figure 1.
99.999% pure chromium pellet imbedded in silver, direct-jet watercooled on the rear target face, before (A) and after (B) irradiation by 60 μA of 16 MeV protons for 1 h.

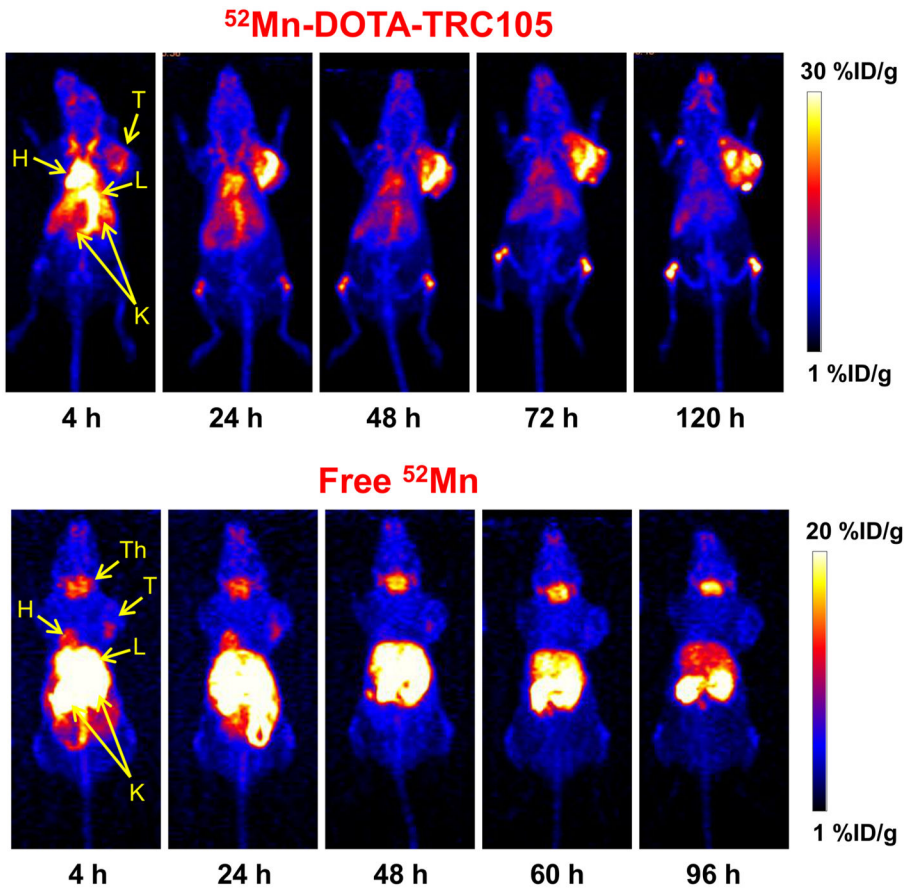

Figure 2.

Serial maximum intensity projection (MIP) PET images of mice injected with ^{52}Mn-DOTA-TRC105 and $^{52}MnCl_2$. Significant thyroid accumulation in the $^{52}MnCl_2$ images contrasting the lack of uptake in the ^{52}Mn-DOTA-TRC105 images indicates highly stable DOTA chelation of $^{52}Mn^{2+}$ even at late time-points. Note: H, Heart; L, Liver; K, Kidneys; T, Tumor; Th, Thyroid.

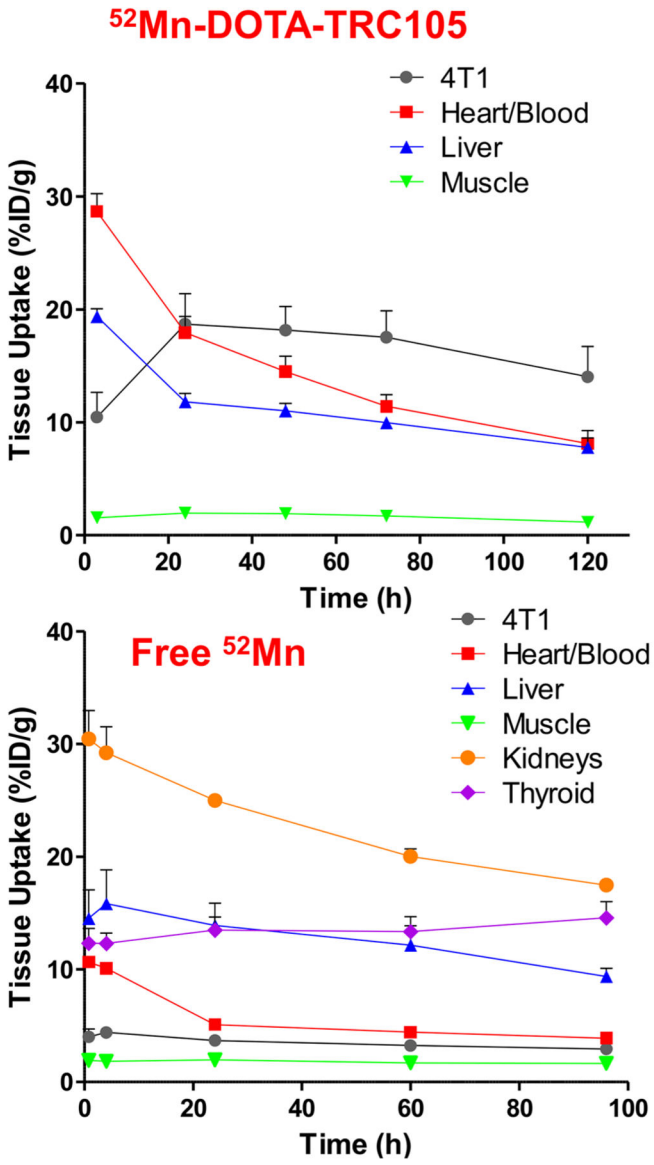

Figure 3.

Time activity curves (TACs) acquired from ROI analysis of PET images obtained in subjects injected with ^{52}Mn-DOTA-TRC105 (n = 3) and with Free ^{52}Mn (n = 4). Error bars represent the standard deviation, and are displayed one-sided for visual clarity. The Heart/Blood TAC uses an ROI drawn over the left ventricle and does not differentiate myocardium from the blood pool.

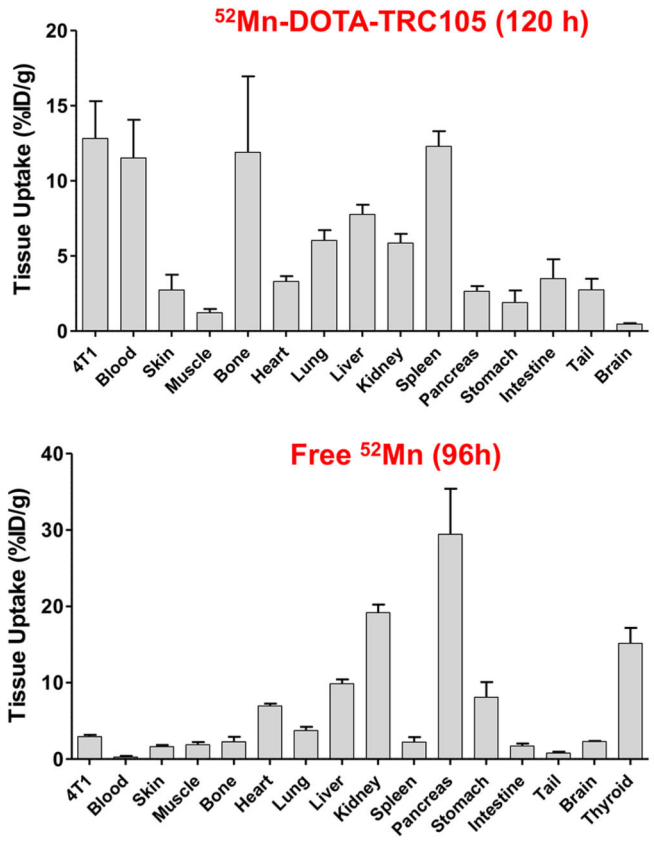

Figure 4.

Ex vivo ^{52}Mn-DOTA-TRC105 (n = 3) and $^{52}MnCl_2$/^{52}Mn-acetate (n = 4) biodistribution data obtained following the last PET time point. Animals were sacrificed, and tissue samples were isolated, washed with saline, dried, weighed, and gamma counted.

Table 1

Stepwise Chromium Reduction in a Single Production Batch Quantified by MP-AES Hold-Back Measurements

	Cr mass (μg)	step separation factor	cumulative separation factor
dissolved target	$(4.05 \pm 0.04) \times 10^3$	-	-
after col. #1	360 ± 18	601 ± 31	$(6.0 \pm 0.3) \times 10^2$
after col. #2	3.82 ± 0.19	80 ± 6	$(4.8 \pm 0.4) \times 10^4$
after col. #3	0.083 ± 0.008	42 ± 5	$(2.0 \pm 0.3) \times 10^6$

Table 2

Trace Metal Analysis by Microwave Plasma Atomic Emission Spectrometry of the Radiochemically Separated ^{52}Mn Product from Approximately 400 mg Dissolved Cr Target Material in Three Independent Separations (A,B,C)

element	A (μg)	B (μg)	C (μg)
Cr	1.07 ± 0.10	0.17 ± 0.02	0.11 ± 0.01
Mn	0.11 ± 0.01	0.23 ± 0.05	0.19 ± 0.01
Fe	0.19 ± 0.02	1.26 ± 0.17	0.72 ± 0.08
Co	0.00 ± 0.01	0.00 ± 0.04	0.00 ± 0.15
Ni	0.00 ± 0.01	0.56 ± 0.16	0.18 ± 0.01
Cu	0.14 ± 0.01	0.04 ± 0.02	0.43 ± 0.06
Zn	3.30 ± 0.33	1.78 ± 0.27	1.10 ± 0.23

Table 3

Radiolabeling Efficiency of ^{52}Mn-DOTA-TRC105 as a Function of Antibody Mass and Time as Measured by Thin Layer Chromatography[a]

mAb mass (μg/MBq)	20 min	40 min	60 min
2.7	85%	89%	95%
6.8	98%	93%	99%
13.5	99%	95%	98%
27.0	99%	93%	100%

[a]Reactions took place at 37 °C in a pH 4.0–4.5 NaOAc buffered solution.